A positive and asymptotic preserving finite volume scheme for the linear transport equation on two dimensional unstructured meshes

Clément Lasuen

A positive and asymptotic preserving finite volume scheme for the linear transport equation on two dimensional unstructured meshes

Clément Lasuen[1]

[1]CEA, DAM, DIF, F-91297 Arpajon, France

clement.lasuen@gmail.com

January 14, 2025

Abstract

In this paper, we propose a finite volume scheme for the linear transport equation in two space dimensions. This scheme is based on an upwind scheme where the velocity is modified so as to recover the correct diffusion limit. The resulting scheme is *asymptotic preserving*, positive under a classical CFL condition and conservative. We propose a reconstruction procedure so as to make it second order consistent on unstructured polygonal meshes.

Contents

1 Introduction

In this work, we propose a finite volume scheme that discretises the radiative transfer equation (see [MM84]):

$$\frac{1}{c}\partial_t I + \text{div}\ (I\boldsymbol{\omega}) + \sigma^t I = \sigma^s \frac{1}{4\pi}\int_{\mathcal{S}^2} I d\boldsymbol{\omega}' + q. \tag{1}$$

It is a linear Boltzmann type equation. The unknown $I = I(t, \mathbf{x}, \boldsymbol{\omega})$ is the radiative intensity and gives the distribution of photons. It depends on the time variable $t \geq 0$, on the space variable $\mathbf{x} \in \Omega \subset \mathbb{R}^3$ (Ω being the computational domain) and direction $\boldsymbol{\omega} \in \mathcal{S}$, where $\mathcal{S}$ is the unit sphere in $\mathbb{R}^3$. The source term $q = q(t, \mathbf{x}, \boldsymbol{\omega}) \geq 0$ is nonnegative. The scattering cross section is $\sigma^s \geq 0$ and the total cross section is $\sigma^t \geq \sigma^s$. The difference $\sigma^t - \sigma^s = \sigma^a$ is the absorption cross section. We assume here that the speed of light c is equal to 1.

Equation (1) is of great importance in the numerical simulation of inertial confinement fusion (ICF). In these experiments, a small ball of hydrogen (the target) is submitted to intense radiation by laser beams. These laser beams are either pointed directly to the target (direct drive approach), or pointed to gold walls of a hohlraum in which the target is located (indirect drive approach, see Figure 1). These gold walls heat up, emitting X-rays toward the target. The outer layers of the target are heated up, hence ablated. By momentum conservation, the inner part of the target implodes (this is usually called the rocket effect). Hence, the pressure and temperature of the hydrogen inside the target increase, hopefully reaching the thermodynamical conditions for nuclear fusion. This process is summarized in Figure 2. Other possible applications of (1) are radiation hydrodynamics in stellar atmospheres. Of course, the model (1) is over-simplified for these applications as it should, among other things, include a dependence on the frequency. But (1) should be seen as an elementary building block for more realistic models.

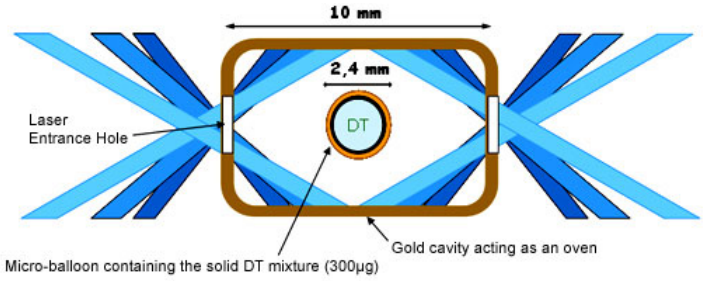

Figure 1: Schematic view of the Hohlraum and the target

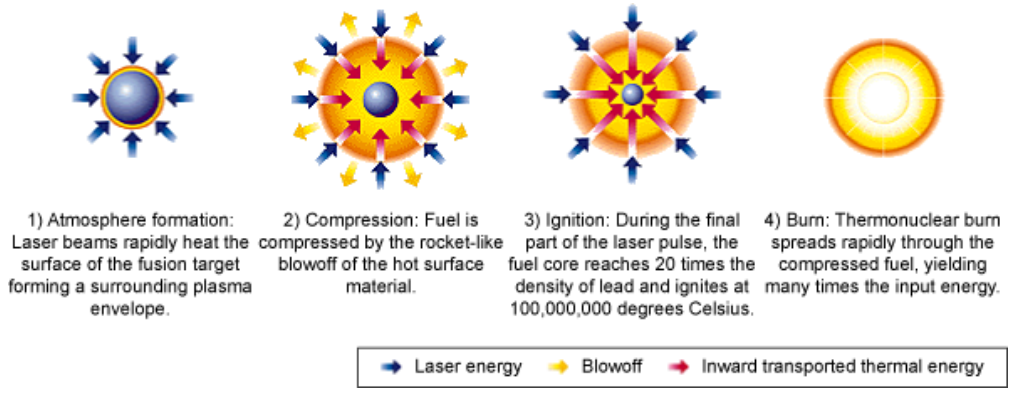

Figure 2: The concept of ICF (inertial confinement fusion) taken from http://www.lanl.gov/projects/dense-plasma-theory/background/dense-laboratory-plasmas.php

It has been shown in [CZ67] that if $q > 0$ and $\sigma^t > 0$ and $\sigma^a > 0$ then the solution I is positive. Moreover, in [RJLM$^+$88] the author proved that if $q = 0$ and $\sigma^t = \sigma^s$ then the solution satisfies a maximum principle property.
Eventually, Equation (1) admits a diffusion limit. Let $\varepsilon > 0$ be given. If we replace $\sigma^s \leftarrow \sigma^s/\varepsilon$, $\sigma^a \leftarrow \sigma^a\varepsilon$, $q \leftarrow q\varepsilon$ and if we perform the following scaling $t \leftarrow \varepsilon t$, then (1) reads as:

$$\partial_t I + \frac{1}{\varepsilon}\text{div }(I\boldsymbol{\omega}) + \frac{\sigma^t}{\varepsilon^2} I = \frac{\sigma^s}{\varepsilon^2}\frac{1}{4\pi}\int_{\mathcal{S}^2} I d\boldsymbol{\omega}' + q, \tag{2}$$

with $\sigma^t = \sigma^s + \varepsilon^2\sigma^a$. Moreover, when ε vanishes, the solution I of (2) converges toward the solution of a diffusion equation $I \xrightarrow[\varepsilon\to 0]{} E^0$ where:

$$\partial_t E^0 - \text{div }\left(\frac{1}{3\sigma^s}\nabla E^0\right) + \sigma^a E^0 = \frac{1}{4\pi}\int_{\mathcal{S}^2} q d\boldsymbol{\omega}'. \tag{3}$$

See [BGPS88] [Cas04]. Therefore it is important for a numerical scheme that discretises (2) to be consistent with the limit model (3). In this case, we say that the scheme is *asymptotic-preserving*. More precisely, the parameter $\varepsilon \in [0, 1]$ characterizes the proportion between the streaming and diffusion phenomena. The configuration $\varepsilon = 1$ corresponds to the free streaming regime and $\varepsilon = 0$ to the pure diffusion regime. We use the notations of Figure 3 and we denote by h the discretisation parameter. The general model (2) is denoted by P^ε and it is discretised with the scheme P_h^ε. The model P^ε tends towards the diffusion limit model P^0 (Equation (3)) when $\varepsilon \to 0$. We want the limit scheme P_h^0 (obtained by setting $\varepsilon \to 0$ in P_h^ε) to be consistent with P^0. If this property is fulfilled, then we say that the scheme P_h^ε is *asymptotic preserving* or *AP*. We emphasize that ε is present in the equations through ε^{-1}, hence the corresponding terms are stiff in the diffusion limit ($\varepsilon \to 0$). The diffusion limit is thus a singular limit. This explains both why the limit equation is of different nature and why designing AP schemes is not trivial.

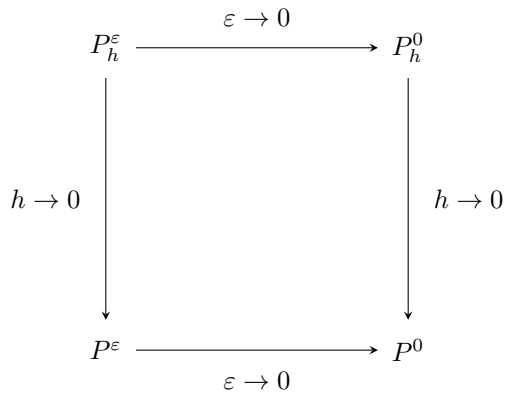

Figure 3: Definition of an AP scheme.

The very first works in this direction were [LMM87] and [JL96]. These papers were dedicated to $1D$ calculations. One dimensional finite difference methods that solved (2) were proposed in [Kla98, JPT00] for instance. The work [KFJ16] proposes an extension of these methods to the two dimensional case. The space and angular variable are both discretised on uniform grids and a time splitting discretisation method (IMEX method, see for instance [BFR16, BR09, EG23]) is performed.
The discontinuous finite elements method was also used to solve (2) on two and three dimensional unstructured meshes. See [Ada01] [BCWA] [CS16] for instance. These methods are consistent but not positive. A recent work [GPR20] proposes a positive, AP and first order scheme to solve the stationary version of (2).
Micro-macro decompositions were also used to solve (2) on uniform grids. See for instance [LFH19, LM08, LM10, JS10, EHW21]. Recently, [ACE$^+$22] proposed an AP finite volume scheme that is based on a micro-macro decomposition. The scheme is first order consistent on $2D$ unstructured meshes but it is not positive.

In this paper we propose a method that:

- is asymptotic preserving: the scheme we obtain when $\varepsilon \to 0$ is consistent with (3),
- is second order consistent on unstructured $2D$ meshes for any ε,
- preserves the positivity of the numerical solution under a classical CFL condition, that is to say $\Delta t = O(h)$ in the streaming regime and $\Delta t = O(h^2)$ in the diffusion regime,
- has a compact stencil,
- is conservative,
- has the same computational cost as an explicit scheme: there is no linear system to invert nor fixed-point iteration to compute.

We perform an angular discretisation of (2). We choose K directions $(\boldsymbol{\omega}_k)_{1\leq k\leq K}$ and we define $I_k = I(t, \mathbf{x}, \boldsymbol{\omega}_k)$ for $1 \leq k \leq K$. The integral over the unit sphere in (2) is discretised as:

$$\frac{1}{4\pi}\int_{\mathcal{S}^2} I d\boldsymbol{\omega}' \approx \sum_{k'=1}^{K} p_{k'} I_{k'}.$$

The quadrature weights $(p_k)_{1\leq k\leq K}$ and the directions $(\boldsymbol{\omega}_k)_{1\leq k\leq K}$ are required to satisfy:

$$p_k \geq 0, \qquad \sum_{k'=1}^{K} p_{k'} = 1, \qquad \sum_{k'=1}^{K} p_{k'}\boldsymbol{\omega}_{k'} = \mathbf{0}. \tag{4}$$

The equation we solve therefore reads as:

$$\partial_t I_k + \frac{1}{\varepsilon}\text{div }(I_k\boldsymbol{\omega}_k) + \frac{\sigma^t}{\varepsilon^2} I_k = \frac{\sigma^s}{\varepsilon^2}\sum_{k'=1}^{K} p_{k'} I_{k'} + q_k. \tag{5}$$

Moreover, owing to (4), when ε vanishes, Equation (5) admits a diffusion limit: $I_k \xrightarrow[\varepsilon\to 0]{} E^0$ where E^0 is solution to (3).
In this work, we focus on the two dimensional case. We briefly explain in the conclusion that our methodology can be easily extended to the three dimensional case.

The main idea of our method is to use an upwind scheme to discretise Equation (5) and to modify the streaming velocity in order to obtain a scheme that is consistent with (3) when $\varepsilon \to 0$. The fluxes are computed at the edges of the cells.
The article is organized as follows. In Section 2, we define the notations that we use in the rest of the paper. Section 3 is dedicated to the numerical scheme and its properties. Numerical examples are shown in Section 4.

2 Notations

We present here some notations that will be used in the rest of the paper. We consider a mesh $\mathcal{T}$ paving the domain Ω. The mesh is made of general polygonal cells. Let $\Omega_j \in \mathcal{T}$ be a cell of the mesh. We define:

- V_j is the volume of the cell Ω_j;
- $\mathbf{x}_j$ is the barycenter of the cell Ω_j;
- $\mathbf{e}$ is an edge of Ω_j and $\mathbf{n}_j^{\mathbf{e}}$ is the outgoing unit normal vector to $\mathbf{e}$ and $|\mathbf{e}|$ is its length;
- $r_1^{\mathbf{e}}$ and $r_2^{\mathbf{e}}$ are the indexes of the nodes of $\mathbf{e}$, and $\mathbf{x}_{r_1^{\mathbf{e}}}$ and $\mathbf{x}_{r_2^{\mathbf{e}}}$ are their coordinates;
- $\mathbf{x}_e$ is the middle of the edge, it is given by $\mathbf{x}_e = (\mathbf{x}_{r_1^{\mathbf{e}}} + \mathbf{x}_{r_2^{\mathbf{e}}})/2$;
- $\sum_{\mathbf{e}\in\Omega_j}$ the sum over all edges of the cell j;

- $N_j = \sum_{\mathbf{e}\in\Omega_j} 1$ the number of edges in the cell Ω_j;
- $\sum_{i|r\in\Omega_i}$ the sum, for a node with index r, over all the cells that contains this node;
- $N_r = \sum_{i|r\in\Omega_i} 1$ the number of cells that contains the given node r;
- $\sum_{j\in\mathcal{T}}$ the sum over all the cells of the mesh;
- $J = \sum_{j\in\mathcal{T}} 1$ is the number of cells of the mesh;
- h the maximum length of edges of the mesh;
- $I_{k,j}^n$ is the value of the unknown in direction k, in cell j, at iteration n;
- $I_k = (I_{k,i})_{i\in\mathcal{T}}$ is the vector of the values of the unknown in direction k;
- $E_j = \sum_{k'=1}^K p_{k'} I_{k',j}$ is the average, in cell j, over the directions;
- $E = (E_i)_{i\in\mathcal{T}}$ is the vector of the averages;
- $\langle\cdot,\cdot\rangle$ the inner product in $\mathbb{R}^2$.

We assume that there exists a constant $C_1 \geq 1$ such that, for any cell j and for any node r:

$$\frac{1}{C_1}h^2 \leq V_j \leq C_1 h^2, \qquad N_j \leq C_1, \qquad N_r \leq C_1. \tag{6}$$

3 Numerical scheme

In this Section we present our numerical scheme. The space discretisation is given in Sections 3.1 and 3.2. The time discretisation is described in 3.3. The properties and the diffusion limit of the scheme are given in Section 3.4 and Section 3.5.

3.1 Upwind scheme and modified streaming velocity

Equation (5) is integrated over the cell Ω_j. Denoting by $I_{k,j}$ the average value of I_k in cell j, we get:

$$\frac{d}{dt}I_{k,j} + \frac{1}{V_j}\int_{\partial\Omega_j} I_k \langle \boldsymbol{\omega}_k, \mathbf{n}\rangle d\mathbf{x} + \frac{\sigma_j^t}{\varepsilon^2} I_{k,j} = \frac{\sigma_j^s}{\varepsilon^2}\sum_{k'=1}^K p_{k'} I_{k',j} + q_{k,j}.$$

The flux is approximated as a sum over the edges of Ω_j:

$$\int_{\partial\Omega_j} I_k \langle \boldsymbol{\omega}_k, \mathbf{n}\rangle d\mathbf{x} \approx \sum_{\mathbf{e}\in\Omega_j} |\mathbf{e}| I_{k,\mathbf{e}} \langle \bar{\boldsymbol{\omega}}_{k,\mathbf{e}}, \mathbf{n}_j^{\mathbf{e}}\rangle,$$

where the streaming velocity $\bar{\boldsymbol{\omega}}_{k,\mathbf{e}}$ is a consistent approximation of $\boldsymbol{\omega}_k/\varepsilon$ that is given below. The edge values $I_{k,\mathbf{e}}$ are computed with an upwind scheme:

$$I_{k,\mathbf{e}} = \begin{cases} I_{k,j} & \text{if } \langle \bar{\boldsymbol{\omega}}_{k,\mathbf{e}}, \mathbf{n}_j^{\mathbf{e}}\rangle > 0, \\ I_{k,i} & \text{else,} \end{cases} \tag{7}$$

where i is the neighboring cell, that is to say, the other cell that contains the edge $\mathbf{e}$, see Figure 4.

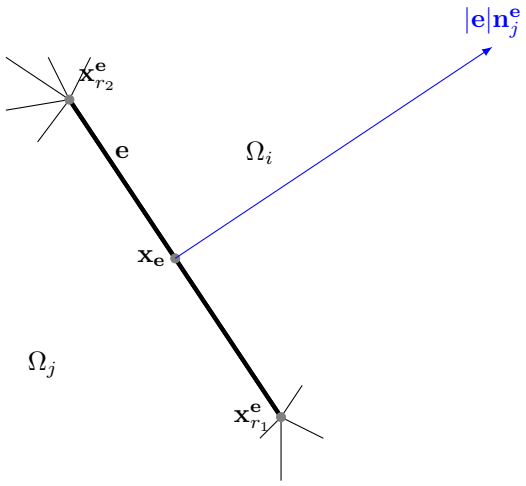

Figure 4: The cells Ω_j and Ω_k share the edge $\mathbf{e}$

The streaming velocity $\bar{\boldsymbol{\omega}}_{k,\mathbf{e}}$ is a consistent approximation of $\boldsymbol{\omega}_k/\varepsilon$, meaning that:

$$\bar{\boldsymbol{\omega}}_{k,\mathbf{e}} = \frac{1}{\varepsilon}\boldsymbol{\omega}_k + O(h^2). \tag{8}$$

We want $\bar{\boldsymbol{\omega}}_{k,\mathbf{e}}$ to be second order consistent with $\boldsymbol{\omega}_k/\varepsilon$ because we aim at designing a scheme that is second order consistent with (5). Moreover, in order to be consistent with (3) in the diffusion regime, we also impose the following condition:

$$\lim_{\varepsilon\to 0} \bar{\boldsymbol{\omega}}_{k,\mathbf{e}} \quad \text{is consistent with} \quad -\frac{\nabla E}{3\sigma^s E}, \tag{9}$$

where E is the average over the directions (see Section 2): $E = \sum_{k'=1}^{K} I_{k'}/K$. The condition (9) is justified in Section 3.5. Therefore we propose:

$$\bar{\boldsymbol{\omega}}_{k,\mathbf{e}} = \frac{\varepsilon^2\boldsymbol{\omega}_k + \left(\sigma_{\mathbf{e}}^t\right)^2 h^3 \mathbf{u}_{\mathbf{e}}}{\varepsilon^3 + (\sigma_{\mathbf{e}}^t h)^3}. \tag{10}$$

The quantity $\mathbf{u}_{\mathbf{e}}$ is an approximation of $-\nabla E/(3E)$ at point $\mathbf{x}_{\mathbf{e}}$. It is given by:

$$\mathbf{u}_{\mathbf{e}} = \frac{\mathbf{u}_{r_1^{\mathbf{e}}} + \mathbf{u}_{r_2^{\mathbf{e}}}}{2},$$

where $\mathbf{u}_{r_1^{\mathbf{e}}}$ and $\mathbf{u}_{r_2^{\mathbf{e}}}$ are approximations of $-\nabla E/(3E)$ at the vertices $\mathbf{x}_{r_1^{\mathbf{e}}}$ and $\mathbf{x}_{r_2^{\mathbf{e}}}$. We choose the formula from [BHL24]. For a given vertex of index r, we set:

$$\mathbf{u}_r = \frac{1}{3E_r}\beta_r^{-1}\sum_{i|r\in\Omega_i} E_i\mathbf{C}_i^r, \qquad E_r = \frac{1}{N_r}\sum_{i|r\in\Omega_i} E_i + h^2, \qquad \beta_r = \sum_{i|r\in\Omega_i} \mathbf{C}_i^r \otimes (\mathbf{x}_r - \mathbf{x}_i), \tag{11}$$

where the node vector $\mathbf{C}_j^r$ is defined as:

$$\mathbf{C}_j^r = \frac{1}{2}\left(|\mathbf{e}_{j,r,1}|\mathbf{n}_j^{\mathbf{e}_{j,r,1}} + |\mathbf{e}_{j,r,2}|\mathbf{n}_j^{\mathbf{e}_{j,r,2}}\right), \tag{12}$$

where $\mathbf{e}_{j,r,1}$, $\mathbf{e}_{j,r,2}$ are the edges of the cell Ω_j that contain the node r. See Figure 5. This definition was first introduced in [CDDL09].

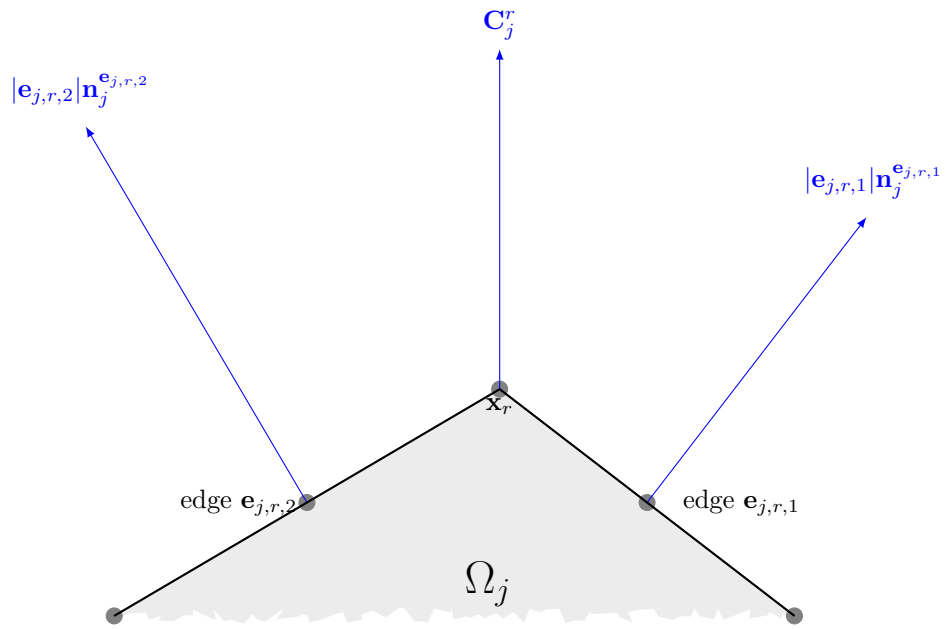

Figure 5: Definition of the node-located vector $\mathbf{C}_j^r$

The quantity E_r is an approximation of E at point $\mathbf{x}_r$. We add a h^2 term in order to make $\mathbf{u}_r$ well defined in the case where all the $(E_i)_i$ vanish. It has been proven in [BHL24] that the quantity $\beta_r^{-1}\sum_{i|r\in\Omega_i} E_i\mathbf{C}_i^r$ is indeed a consistent approximation of $-\nabla E$. The following estimate has also been proven:

Lemma 3.1. *If the matrix β_r satisfies the following property:*

$$\forall \boldsymbol{\xi}\in\mathbb{R}^2,\ \langle \beta_r\boldsymbol{\xi},\boldsymbol{\xi}\rangle \geq \frac{1}{C_{13}}h^2\|\boldsymbol{\xi}\|^2. \tag{13}$$

for some constant $C_{13}>0$, and if the $(I_{k,j})_{k\leq K,j\in\mathcal{T}}$ are nonnegative, then we have, for any edge $\mathbf{e}$:

$$\|\mathbf{u}_\mathbf{e}\| \leq \frac{C_1C_{13}}{3h}.$$

Assumption (13) depends on the mesh and it is studied in [Fra12].

Owing to Lemma 3.1, we see that Definition (10) clearly does satisfy (8) and (9). Thus the resulting scheme is nonlinear and second order consistent with (5). Moreover, in the streaming regime, that is to say when $\sigma^t=\sigma^s=0$, we have exactly $\bar{\boldsymbol{\omega}}_{k,\mathbf{e}}=\boldsymbol{\omega}_k/\varepsilon$. We also emphasize that $\bar{\boldsymbol{\omega}}_{k,\mathbf{e}}$ in (10) may be written as a convex combination between the advection velocity $\boldsymbol{\omega}_k/\varepsilon$ and the "diffusion" velocity $\mathbf{u}/\sigma^s$:

$$\bar{\boldsymbol{\omega}}_{k,\mathbf{e}} = \eta\frac{\boldsymbol{\omega}_k}{\varepsilon}+(1-\eta)\frac{\mathbf{u}_\mathbf{e}}{\sigma^s_\mathbf{e}}, \qquad \eta=\frac{\varepsilon^3}{\varepsilon^3+(\sigma^t_\mathbf{e}h)^3}.$$

Remark 1 (Discontinuity of the cross sections)**.** *In the case when σ^t is discontinuous, then we choose the mesh such that the discontinuity is located at an interface $\mathbf{e}^*$. At this interface, σ^t is no longer defined. To overcome this difficulty, we set, at this interface:*

$$\bar{\boldsymbol{\omega}}_{k,\mathbf{e}^*}=\frac{\boldsymbol{\omega}_k}{\varepsilon}.$$

3.2 Second order fluxes

So far the approximation of the flux is only first order consistent. We use here the procedure from [BHL24] so as to make it second order consistent. Instead of computing the upwind values with (7), we set:

$$I_{k,\mathbf{e}} = \begin{cases} \bar{I}^{\mathbf{e}}_{k,j} & \text{if } \langle \bar{\boldsymbol{\omega}}_{k,\mathbf{e}}, \mathbf{n}^{\mathbf{e}}_j \rangle > 0, \\ \bar{I}^{\mathbf{e}}_{k,i} & \text{else,} \end{cases} \tag{14}$$

where i is the neighboring cell (see Figure 4). The quantity $\bar{I}^{\mathbf{e}}_{k,j}$ is a second order approximation of I_k at point $\mathbf{x}_\mathbf{e}$ in cell j that is given by:

$$\bar{I}^{\mathbf{e}}_{k,j} = \begin{cases} I_{k,j} - \langle \mathbf{g}_{k,\mathbf{e}}, \mathbf{x}_j - \mathbf{x}_\mathbf{e} \rangle & \text{if } |\langle \mathbf{g}_{k,\mathbf{e}}, \mathbf{x}_j - \mathbf{x}_\mathbf{e} \rangle| < I_{k,j}, \\ I_{k,j} \qquad \text{else.} \end{cases} \tag{15}$$

The vector $\mathbf{g}_{k,\mathbf{e}}$ is an approximation of $-\nabla I_k$ at point $\mathbf{x}_\mathbf{e}$. It is computed as:

$$\mathbf{g}_{k,\mathbf{e}} = \frac{\mathbf{g}_{k,r_1} + \mathbf{g}_{k,r_2}}{2}, \qquad \mathbf{g}_{k,r} = \beta_r^{-1} \sum_{i | r \in \Omega_i} I_{k,i} \mathbf{C}^r_i. \tag{16}$$

Defining:

$$\mathcal{F}_{k,j} = \frac{1}{V_j} \sum_{\mathbf{e} \in \Omega_j} |\mathbf{e}| I_{k,\mathbf{e}} \langle \bar{\boldsymbol{\omega}}_{k,\mathbf{e}}, \mathbf{n}^{\mathbf{e}}_j \rangle,$$

the scheme reads as:

$$\frac{d}{dt} I_{k,j} + \mathcal{F}_{k,j} + \frac{\sigma^t_j}{\varepsilon^2} I_{k,j} = \frac{\sigma^s_j}{\varepsilon^2} \sum_{k'=1}^{K} p_{k'} I_{k',j} + q_{k,j}.$$

3.3 Partially implicit time discretisation

We use a partially implicit time discretisation. The streaming term is chosen completely explicit whilst the source and absorption terms are still implicit:

$$\frac{I^{n+1}_{k,j} - I^n_{k,j}}{\Delta t} + \mathcal{F}^n_{k,j} + \frac{\sigma^t_j}{\varepsilon^2} I^{n+1}_{k,j} - \frac{\sigma^s_j}{\varepsilon^2} \sum_{k'=1}^{K} p_{k'} I^{n+1}_{k',j} = q_{k,j} \tag{17}$$

Owing to Sherman-Morrison Lemma 3.2, we can write an explicit formula for $I^{n+1}_{k,j}$. This result is given in Proposition 3.3. Besides, it shows that System (17) can be written as a system without any stiff term. Thus, this system admits a finite and nonzero limit when $\varepsilon \to 0$. This limit is described in Section 3.5.

Lemma 3.2. *Let $A \in \mathbb{R}^{K \times K}$ be nonsingular, and let $u \in \mathbb{R}^K$, $v \in \mathbb{R}^K$. The matrix $A + u \otimes v$ is nonsingular if and only if $1 + \langle v, A^{-1} u \rangle \neq 0$. Besides, in such a case, its inverse is given by:*

$$(A + u \otimes v)^{-1} = A^{-1} - \frac{1}{1 + \langle v, A^{-1} u \rangle} A^{-1} u \otimes v A^{-1}. \tag{18}$$

Proof. The proof can be found in [Ser02]. □

Proposition 3.3. *Equation (17) is equivalent to:*

$$I^{n+1}_{k,j} = \mu^{(1)}_j \left(I^n_k - \Delta t \mathcal{F}^n_{k,j} + \Delta t q_{k,j} \right) + \mu^{(2)}_j \sum_{k'=1}^{K} p_{k'} \left(I^n_{k',j} - \Delta t \mathcal{F}^n_{k',j} + \Delta t q_{k',j} \right), \tag{19}$$

where:

$$\mu^{(1)}_j = \frac{\varepsilon^2}{\varepsilon^2 + \Delta t \sigma^t_j}, \qquad \mu^{(2)}_j = \frac{\Delta t \sigma^s_j}{\varepsilon^2 + \Delta t \sigma^t_j} \times \frac{1}{1 + \Delta t \sigma^a_j}. \tag{20}$$

Proof. Using (20), Equation (17) reads as:

$$I_{k,j}^{n+1} - \frac{\Delta t \sigma_j^s}{\varepsilon^2 + \Delta t \sigma_j^t} \sum_{k'=1}^{K} p_{k'} I_{k',j}^{n+1} = \mu_j^{(1)} \left(I_k^n - \Delta t \mathcal{F}_{k,j}^n + \Delta t q_{k,j} \right). \tag{21}$$

Equation (21) can be set under the following form:

$$\left(i_K - \lambda_j v \otimes p\right) I_j^{n+1} = b_j, \qquad I_j^{n+1} = \begin{pmatrix} I_{1,j}^{n+1} \\ \vdots \\ I_{K,j}^{n+1} \end{pmatrix} \in \mathbb{R}^K, \qquad p = \begin{pmatrix} p_1 \\ \vdots \\ p_K \end{pmatrix} \in \mathbb{R}^K, \qquad v = \begin{pmatrix} 1 \\ \vdots \\ 1 \end{pmatrix} \in \mathbb{R}^K, \tag{22}$$

where i_K is the identity matrix of size K and:

$$\lambda_j = \frac{\Delta t \sigma_j^s}{\varepsilon^2 + \Delta t \sigma_j^t}, \qquad b_{k,j} = \mu_j^{(1)} \left(I_k^n - \Delta t \mathcal{F}_{k,j}^n + \Delta t q_{k,j} \right).$$

Moreover, owing to (4), we have:

$$1 - \lambda_j \langle v, p \rangle = 1 - \frac{\Delta t \sigma_j^s}{\varepsilon^2 + \Delta t \sigma_j^t} > 0.$$

Therefore, according to Lemma 3.2, the matrix of System (22) is nonsingular and its inverse is given by:

$$\left(i_K - \lambda_j v \otimes p\right)^{-1} = i_K + \frac{\lambda_j}{1 - \frac{\Delta t \sigma_j^s}{\varepsilon^2 + \Delta t \sigma_j^t}} v \otimes p = i_K + \frac{\Delta t \sigma_j^s}{\varepsilon^2 + \Delta t \varepsilon^2 \sigma_j^a} v \otimes p.$$

Thus Equation (21) becomes:

$$I_{k,j}^{n+1} = \mu_j^{(1)} \left(I_k^n - \Delta t \mathcal{F}_{k,j}^n + \Delta t q_{k,j} \right) + \underbrace{\mu_j^{(1)} \frac{\Delta t \sigma_j^s}{\varepsilon^2 + \Delta t \varepsilon^2 \sigma_j^a}}_{= \mu_j^{(2)}} \sum_{k'=1}^{K} p_{k'} \left(I_{k',j}^n - \Delta t \mathcal{F}_{k',j}^n + \Delta t q_{k',j} \right).$$

The result is proved.

□

Therefore $I_{k,j}^{n+1}$ writes explicitly as a function of the quantities at iteration n. Besides, if $q = \sigma^a = 0$ then $\mu_j^{(1)} + \mu_j^{(2)} = 1$ and $I_{k,j}^{n+1}$ simply reads as a convex combination between the anisotropic and isotropic dynamics. We observe in Section 4 that the scheme (19) is indeed second order convergent. Moreover, the positivity of the solution is preserved under a classical CFL condition (see Proposition 3.6 below).

Remark 2. *The scheme* (19) *has the same computational cost as an explicit scheme. There is no stiff term. No fixed point iteration is required, no linear system needs to be solved. Thus each time iteration is very fast to compute and there is no need for an acceleration procedure in the diffusion limit.*

3.4 Properties

In this section, we present the properties of the scheme (17). We first detail the conservation property (Proposition 3.4), then we give an intermediary result (Lemma 3.5) that is used in the proof of the CFL condition (Proposition 3.6). The proofs can be found in Appendix 6.

Proposition 3.4. *We assume periodic boundary conditions are imposed. If $\sigma^a = 0$, then the scheme* (17) *is conservative:*

$$\sum_{j \in \mathcal{T}} V_j E_j^{n+1} = \sum_{j \in \mathcal{T}} V_j E_j^n + \Delta t \sum_{j \in \mathcal{T}} V_j \sum_{k'=1}^{K} p_{k'} q_{k',j}.$$

Lemma 3.5. *Under the assumptions of Lemma 3.1, there exists a constant $C_{3.5}$ such that, for any edge* $\mathbf{e}$ *and any direction* k*:*

$$\|\bar{\boldsymbol{\omega}}_{k,\mathbf{e}}\| \leq \frac{C_{3.5}}{\sigma^t_{\mathbf{e}} h + \varepsilon}.$$

Proposition 3.6. *Under the assumptions of Lemma 3.1 and if* (6) *is fulfilled, there exists a constant* $C_{3.6} > 0$ *such that, if* $\left(I^n_{k,j}\right)_{k,j}$ *and* q *are nonnegative, and if:*

$$\Delta t \leq C_{3.6}\left(\varepsilon h + h^2 \min_{\mathbf{e}\in\mathcal{T}} \sigma^t_{\mathbf{e}}\right), \tag{23}$$

then $I^{n+1}_{k,j}$ *is nonnegative for all* k, j*.*

3.5 AP property and limit scheme

In this Section, we explain why the scheme (19) is AP. More precisely, we study the limit of the scheme (19) as ε goes to 0. First, one can easily see that:

$$\mu^{(1)}_j \xrightarrow[\varepsilon\to 0]{} 0. \tag{24}$$

Besides, using $\sigma^t = \sigma^s + \varepsilon^2\sigma^a$ leads to:

$$\mu^{(2)}_j \xrightarrow[\varepsilon\to 0]{} \frac{1}{1+\Delta t\sigma^a}. \tag{25}$$

Therefore, combining (19) and (24) (25) gives the following limit as ε vanishes:

$$I^{n+1}_{k,j} = \frac{1}{1+\Delta t\sigma^a}\sum_{k'=1}^{K} p_{k'}\left(I^n_{k',j} - \Delta t\mathcal{F}^n_{k,j} + \Delta t q_{k',j}\right).$$

Thus I is isotropic:

$$I^{n+1}_{k,j} = \sum_{k'=1}^{K} p_{k'} I^{n+1}_{k',j} = E^{n+1}_j.$$

In addition, when ε vanishes, the velocity field does not depend on ω_k anymore ans so is the flux:

$$\bar{\boldsymbol{\omega}}_{k,\mathbf{e}} = \frac{\mathbf{u}_{\mathbf{e}}}{\sigma^s_{\mathbf{e}}}, \qquad \mathcal{F}_{k,j} = \frac{1}{V_j}\sum_{\mathbf{e}\in\Omega_j} |\mathbf{e}| E_{\mathbf{e}} \left\langle \frac{\mathbf{u}_{\mathbf{e}}}{\sigma^s_{\mathbf{e}}}, \mathbf{n}^{\mathbf{e}}_j \right\rangle =: \mathcal{F}_j.$$

Therefore, as ε goes to 0, Equation (19) becomes:

$$(1+\Delta t\sigma^a)E^{n+1}_j = E^n_j - \Delta t\mathcal{F}^n_j + \Delta t\sum_{k'=1}^{K} p_{k'} q_{k',j},$$

which may be written as:

$$\frac{E^{n+1}_j - E^n_j}{\Delta t} + \mathcal{F}^n_j + \sigma^a_j E^{n+1}_j = \sum_{k'=1}^{K} p_{k'} q_{k',j}. \tag{26}$$

As $\mathbf{u}$ is consistent with $-\nabla E/3E$, the flux $\mathcal{F}_j$ is consistent with $-\text{div}\,(E\times\nabla E/3\sigma^s E) = -\text{div}\,(\nabla E/(3\sigma^s)$. Therefore (26) is consistent with (3). It is the second order scheme from [BHL24].

3.6 Dirichlet boundary conditions

We denote by $\gamma \in \mathcal{C}^0(\partial\Omega \times S^2)$ the Dirichlet boundary condition:

$$I(t, \mathbf{x}, \boldsymbol{\omega}) = \gamma(\mathbf{x}, \boldsymbol{\omega}), \qquad \text{if } \mathbf{x} \in \partial\Omega, \qquad \text{and } \langle \boldsymbol{\omega}, \mathbf{n} \rangle < 0,$$

where $\mathbf{n}$ is normal vector to the boundary of the domain. In the cells on the boundary and for the edges on the boundary, the upwind value (14) is replaced by:

$$I_{k,\mathbf{e}} = \begin{cases} \bar{I}^{\mathbf{e}}_{k,j} & \text{if } \langle \bar{\boldsymbol{\omega}}_{k,\mathbf{e}}, \mathbf{n}^{\mathbf{e}}_j \rangle > 0, \\ \gamma(\mathbf{x}, \boldsymbol{\omega}_k) & \text{else,} \end{cases} \tag{27}$$

Note that the gradients $\mathbf{u}_r$ given by (11) is not well-defined in the corner nodes. Indeed there is only one support cell and thus the matrix β_r has rank 1 and is singular. To overcome this difficulty we compute the gradient $\mathbf{u}_r$ at the corner as the average of the gradients at the other nodes of the support cell.

3.7 Periodic boundary conditions

In the case of periodic boundary conditions, we add some *ghost* cells on the outside of the mesh so as to make it periodic. We then define I on these new cells and we use these values and this new geometric data to compute the $\mathbf{C}^r_j$ on the boundary of the domain.

4 Numerical results

In this Section we present some numerical examples to illustrate the good properties of our method. We use a quadrature of *Equal Weights* from [Car]. The weights $(p_k)_{1 \le k \le K}$ are equal to $1/K$ and the number of directions has to be of the following form $K = 4N^2$ with $N \in \mathbb{N}$.
In the first three test cases, we compute analytical solutions of (2) and we perform a convergence analysis (Sections 4.1, 4.2, 4.3) on cartesian meshes (uniform grids) and random meshes (see Figure 6). Denoting by $\tilde{I}$ the exact solution and t_f the final time, the error is computed the following way:

$$\text{error } = \max_{1 \le k \le K} \left(\frac{\sum_{j \in \mathcal{T}} V_j \left| I_{k,j} - \tilde{I}(t_f, \mathbf{x}_j, \boldsymbol{\omega}_k) \right|}{\sum_{j \in \mathcal{T}} V_j \tilde{I}(t_f, \mathbf{x}_j, \boldsymbol{\omega}_k)} \right).$$

We also compute the solution of a *Lattice problem* defined in [BH05] in Section 4.5. Eventually we present our results for a test case from [KFJ16].

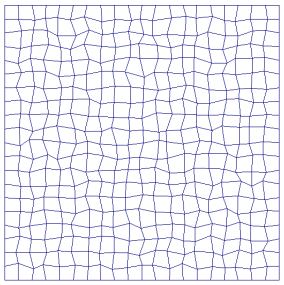

Figure 6: Random mesh.

4.1 Free streaming regime

In this test case, we choose $\sigma^s = \sigma^a = 0$, $q = 0$ and $\varepsilon = 1$. The exact solution is given by:

$$I(t, \mathbf{x}, \boldsymbol{\omega}) = \exp\left(-100 \left\| \mathbf{x} - t\boldsymbol{\omega} - \mathbf{x}_0 \right\|^2 \right), \qquad \mathbf{x}_0 = (1, 1).$$

Dirichlet boundary conditions are imposed (see Section 3.6). We choose $K = 4$ directions. The computational domain is $\Omega = [0, 2]^2$. Figure 7 shows the error curve at final time $t_f = 0.03$ and $\Delta t = h^2$. Indeed, as the scheme (19) is first order consistent in time, we need to set $\Delta t = O(h^2)$ in order to make the consistency error decrease as h^2. We see that our method gives the expected rate of convergence.

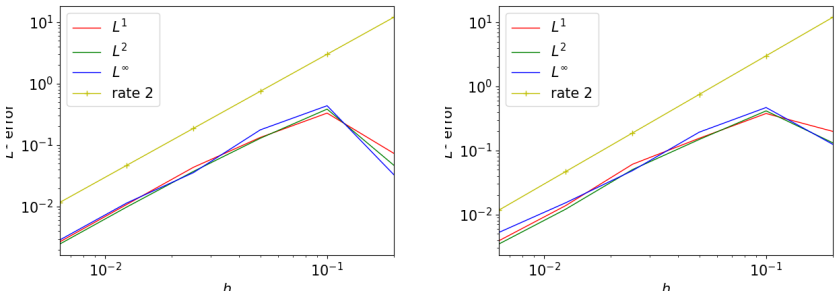

Figure 7: Error on cartesian (left) and random (right) meshes.

4.2 Diffusion regime

In this test case, we choose $\sigma^s = 1$, $\sigma^a = q = 0$ and $\varepsilon = 0$. The exact solution is the fundamental solution of the diffusion equation:

$$\partial_t E - \frac{1}{3}\Delta E = 0, \qquad E(t, \mathbf{x}) = \frac{3}{4\pi(t + t_0)} \exp\left(-3\frac{\|\mathbf{x} - \mathbf{x}_0\|^2}{4(t + t_0)}\right),$$

with $t_0 = 0.01$ and $\mathbf{x}_0 = (1, 1)$. The computational domain is $\Omega = [0, 2]^2$. Periodic boundary conditions are imposed. We choose $K = 4$ directions. The timestep is given by $\Delta t = h^2$ and the final time is $t_f = 0.03$. Figure 8 shows the error curves. The right convergence rate is recovered.

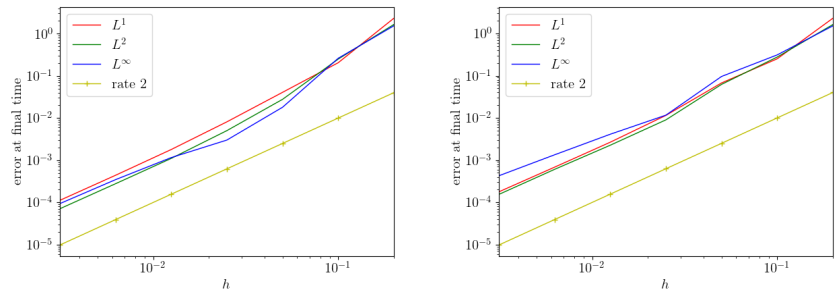

Figure 8: Error on cartesian (left) and random (right) meshes.

4.3 Manufactured test case

We choose $\varepsilon = 1$. The analytical solution of this test case is given by:

$$I(t, x, y, \boldsymbol{\omega}) = e^t \left(10 + \sin(2\pi x) + \sin(2\pi y) + \langle \boldsymbol{\omega}, \mathbf{f} \rangle\right), \qquad \mathbf{f} = (1, -1),$$

and the absorption coefficients are given by:

$$\sigma^t(x, y) = 2 + (\sin(2\pi x) + \sin(2\pi y))^2, \qquad \sigma^s = 0.1.$$

We compute the source term $q(t, x, y, \boldsymbol{\omega})$ so as to satisfy Equation (2). Periodic boundary conditions are imposed. We set $K = 4$. Figure 9 displays the error curves with the second order scheme at time $t_f = 0.01$ and $\Delta t = h^2$.

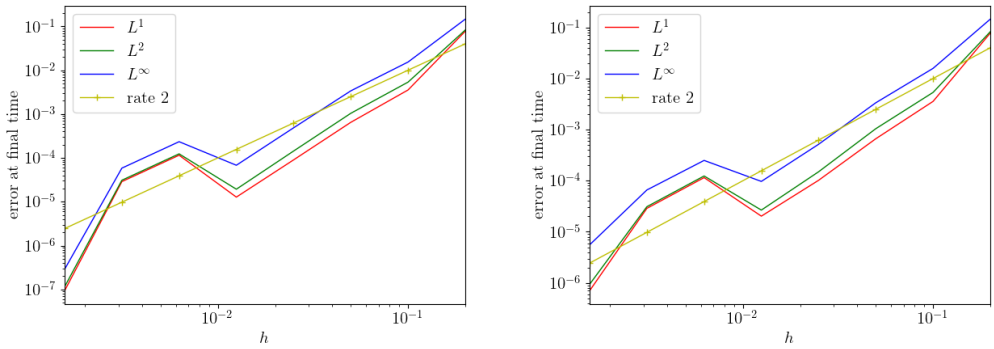

Figure 9: Error on cartesian meshes (left) and random meshes (right).

4.4 Stationary boundary layer

This $1D$ test case is borrowed from [ACE+22]. We set $\varepsilon = 1$ and:

$$q = 1_{|x|\leq 0.1}, \qquad \sigma^a = 1_{|x|\leq 0.8} + 10 \times 1_{1\leq |x|\leq 1.2}, \qquad \sigma^s = 100 \times 1_{0.8\leq |x|\leq 1}.$$

The computational domain is $[-1.2, 1.2]$. The initial and boundary conditions are zero. We solve this test case with a $1D$ version of the scheme. The idea is to compute the long time stationary solution of (2). Besides, due to the strong discontinuity of σ^s at $x = 0.8$, the solution develops a *boundary layer*: the energy is transported until $x = 0.8$, then it accumulates in a neighborhood of the boundary before decreasing exponentially due to the strong opacity. See [lM89] for instance.

Figure 10 shows the solution at time $t_f = 10^8$ with 48 cells, $\Delta t = h$ and $K = 8$ directions. We observe the development of boundary layers when the solution enters the opaque zones at $|x| = 0.8$, as depicted in [ACE+22].

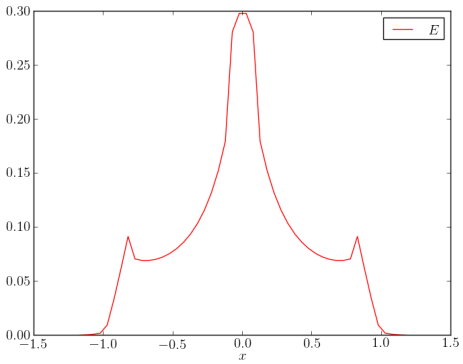

Figure 10: Numerical solution at time $t_f = 10^8$.

4.5 Lattice problem

This test case is borrowed from [BH05]. The computational domain is $\Omega = [0, 7]^2$. The initial condition is 0 and $\varepsilon = 1$. The source term is $q = 1_{[3,4]\times[3,4]}$. Homogeneous Dirichlet boundary conditions are imposed.

The final time is $t_f = 3.2$ and the time step is $\Delta t = 0.01$. The absorption coefficients are:

$$\sigma^t = 10 \times 1_{\Omega_A}, \qquad \sigma^s = 1 - 1_{\Omega_A}.$$

The domain Ω_A is pictured in red color in Figure 11.

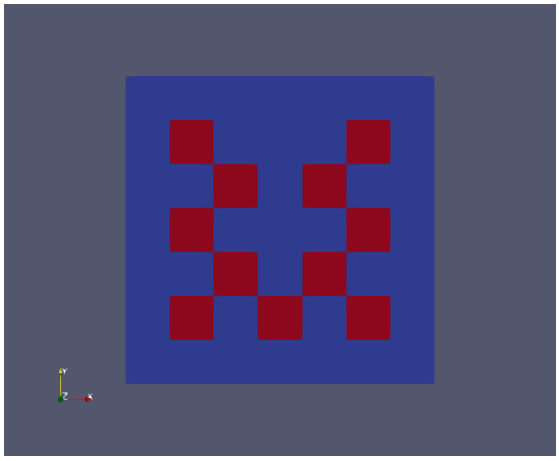

Figure 11: The domain Ω_A in red color.

Some numerical solutions are plotted in the following Figures. The log scale map is limited to seven orders of magnitude: we display with the same blue color all the regions where the solution is smaller or equal to 10^{-7}.

Figures 12, 13 and 14 display the numerical solution with $K = 4$, $K = 144$ and $K = 484$ respectively. We see that we recover the results of [BH05].

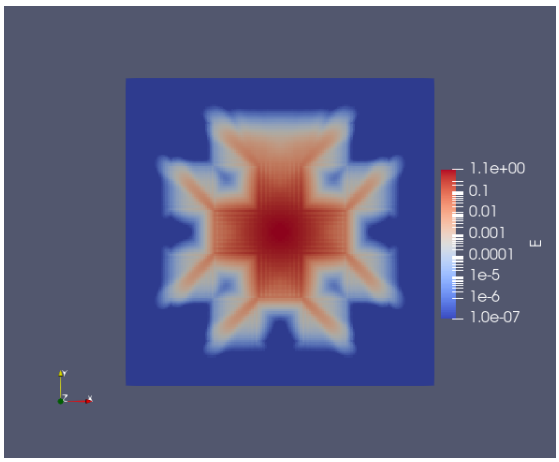

Figure 12: Numerical solution (in log scale) at time $t_f = 3.2$ on a cartesian mesh of size 140×140 and with $K = 4$.

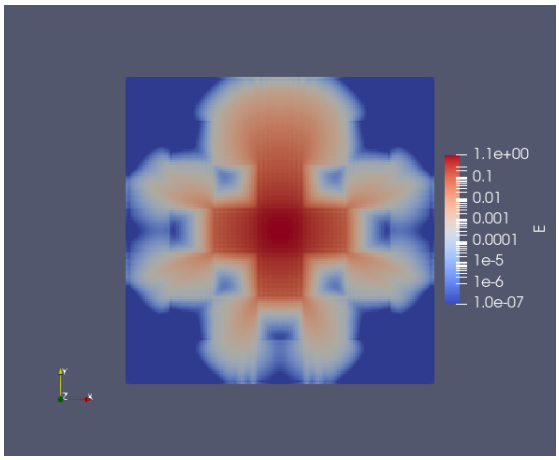

Figure 13: Numerical solution (in log scale) at time $t_f = 3.2$ on a cartesian mesh of size 140×140 and with $K = 144$.

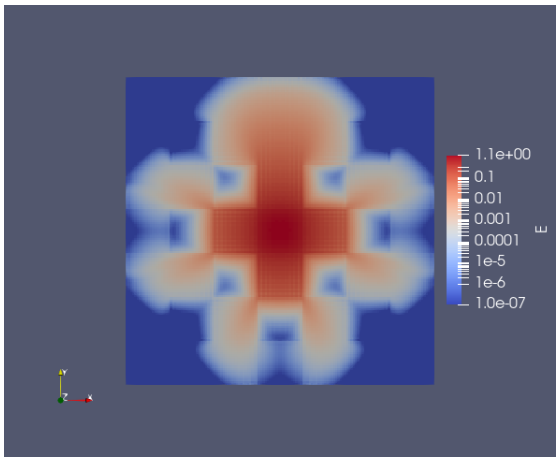

Figure 14: Numerical solution (in log scale) at time $t_f = 3.2$ on a cartesian mesh of size 140×140 and with $K = 484$.

4.6 Variable scattering test case

Here we compute the solution of the *variable scattering* test case from [KFJ16]. The domain is $[-1, 1]^2$, the final time is $t_f = 0.005$ and we set $\varepsilon = 0.01$ and $\sigma^a = q = 0$. The initial condition and the cross section are given by:

$$I(t = 0, x, y, \omega_x, \omega_y) = \frac{1}{0.04\pi} \exp\left(-\frac{x^2 + y^2}{0.04}\right), \qquad \sigma^s(x, y) = \begin{cases} c^4(c^2 - 2)^2 & \text{if } c = \sqrt{x^2 + y^2} < 1, \\ 1 & \text{else.} \end{cases}$$

The solution is almost 0 near the boundary, so we impose periodic boundary conditions. Figure 15 shows the solution E on a uniform grid of size $N_x = N_y = 200$ with $\Delta t = 10^{-3}$. We do recover the solution from [KFJ16].

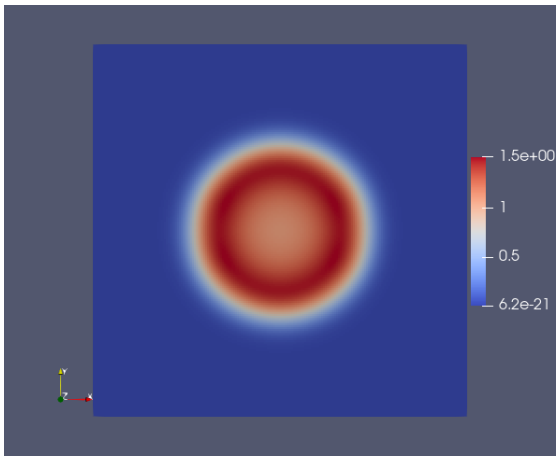

Figure 15: Numerical solution E at time $t_f = 0.005$ on a cartesian mesh of size 200×200 and with $K = 64$.

5 Conclusion and future work

In this paper we have presented a scheme that is asymptotic preserving, positive under a classical CFL condition that depend on the regime, conservative and second order consistent in space. Besides its computational cost is quite low as there is no linear system to solve nor fixed point iteration to compute.

Several extensions to this work are possible. First, the method can be easily adapted to $3D$ unstructured meshes. Indeed, the $3D$ formulas for the node vectors $\left(\mathbf{C}_j^r\right)_{j,r}$ are given in [CDDL09]. In addition, we have seen in Proposition 3.3 that the intensity at iteration $n+1$ can be explicitely computed as a function of the quantities at iteration n. This property will allow us to design a scheme to solve efficiently the transport equation coupled with matter. This is an ongoing work.

6 Appendix

6.1 Proof of Proposition 3.4

We multiply Equation (17) by p_k and we sum over the directions, this gives:

$$\frac{1}{\Delta t}\left[\sum_{k'=1}^{K} p_{k'} I_{k',j}^{n+1} - \sum_{k'=1}^{K} p_{k'} I_{k',j}^{n} - \Delta t \sum_{k'=1}^{K} p_{k'} q_{k',j}\right] + \sum_{k'=1}^{K} p_{k'} \mathcal{F}_j(I_{k'}^n, \bar{\boldsymbol{\omega}}_{k'}^n) = 0. \tag{28}$$

We multiply (28) by V_j and we sum over the cells, which leads to:

$$\frac{1}{\Delta t}\sum_{j\in\mathcal{T}} V_j\left[\sum_{k'=1}^{K} p_{k'} I_{k',j}^{n+1} - \sum_{k'=1}^{K} p_{k'} I_{k',j}^{n} - \Delta t \sum_{k'=1}^{K} p_{k'} q_{k',j}\right] + \sum_{k'=1}^{K} p_{k'} \sum_{j\in\mathcal{T}} V_j \mathcal{F}_{k',j}^n = 0.$$

Now we prove:

$$\sum_{j\in\mathcal{T}} V_j \mathcal{F}_{k,j}^n = 0.$$

We remove the upper-scripts n in order to clarify the algebra. By definition, we have:

$$\sum_{j\in\mathcal{T}} V_j \mathcal{F}_{k,j} = \sum_{j\in\mathcal{T}} \sum_{\mathbf{e}\in\Omega_j} |\mathbf{e}| \left\langle \mathbf{n}_j^{\mathbf{e}}, \bar{\boldsymbol{\omega}}_{k,\mathbf{e}} \right\rangle I_{k,\mathbf{e}}.$$

and:

$$\sum_{j\in\mathcal{T}}\sum_{\mathbf{e}\in\Omega_j}|\mathbf{e}|\left\langle\mathbf{n}_j^{\mathbf{e}},\bar{\boldsymbol{\omega}}_{k,\mathbf{e}}\right\rangle I_{k,\mathbf{e}}=\sum_{\mathbf{e}\in\mathcal{T}}\sum_{i|\mathbf{e}\in i}|\mathbf{e}|\left\langle\mathbf{n}_i^{\mathbf{e}},\bar{\boldsymbol{\omega}}_{k,\mathbf{e}}\right\rangle I_{k,\mathbf{e}},$$

where $\sum_{i|\mathbf{e}\in i}$ denotes the sum, for a given edge $\mathbf{e}$, over the two cells that share this edge. Besides, we have:

$$\sum_{i|\mathbf{e}\in i}|\mathbf{e}|\left\langle\mathbf{n}_i^{\mathbf{e}},\bar{\boldsymbol{\omega}}_{k,\mathbf{e}}\right\rangle I_{k,\mathbf{e}}=|\mathbf{e}|I_{k,\mathbf{e}}\left\langle\bar{\boldsymbol{\omega}}_{k,\mathbf{e}},\underbrace{\sum_{i|\mathbf{e}\in i}\mathbf{n}_i^{\mathbf{e}}}_{=\mathbf{0}}\right\rangle.$$

The result is proved.

6.2 Proof of Proposition 3.5

We use Lemma 3.1 and $\|\boldsymbol{\omega}_k\|\leq 1$ in (10). This gives:

$$\|\bar{\boldsymbol{\omega}}_{k,\mathbf{e}}\|\leq\max\left(1,\frac{C_1C_{13}}{3}\right)\frac{\varepsilon^2+(\sigma_{\mathbf{e}}^t h)^2}{\varepsilon^3+(\sigma_{\mathbf{e}}^t h)^3}\leq 4\max\left(1,\frac{C_1C_{13}}{3}\right)\frac{1}{\sigma_{\mathbf{e}}^t h+\varepsilon}. \tag{29}$$

The result is proved.

6.3 Proof of Proposition 3.6

Let $1\leq k\leq K$. First, we define:

$$R_j^+=\{\mathbf{e}\in\Omega_j,\quad\langle\mathbf{n}_j^{\mathbf{e}},\bar{\boldsymbol{\omega}}_{k,\mathbf{e}}\rangle>0\},\qquad R_j^-=\{\mathbf{e}\in\Omega_j,\quad\langle\mathbf{n}_j^{\mathbf{e}},\bar{\boldsymbol{\omega}}_{k,\mathbf{e}}\leq 0\}.$$

Using these definitions, we easily have:

$$I_{k,j}-\Delta t\mathcal{F}_{k,j}\geq I_{k,j}-\frac{\Delta t}{V_j}\sum_{\mathbf{e}\in\tilde{R}_j^+}|\mathbf{e}|\left\langle\mathbf{n}_j^{\mathbf{e}},\bar{\boldsymbol{\omega}}_{k,\mathbf{e}}\right\rangle I_{k,\mathbf{e}}.$$

According to (15), we have $I_{k,\mathbf{e}}\leq 2I_{k,j}$. This leads to:

$$I_{k,j}-\Delta t\mathcal{F}_{k,j}\geq g_j\left(1-\frac{2\Delta t}{V_j}\sum_{\mathbf{e}\in\tilde{R}_j^+}|\mathbf{e}|\left\langle\mathbf{n}_j^{\mathbf{e}},\bar{\boldsymbol{\omega}}_{k,\mathbf{e}}\right\rangle\right). \tag{30}$$

Besides, using Assumption (6) and Lemma 3.5, we have:

$$\frac{\Delta t}{V_j}\sum_{\mathbf{e}\in\tilde{R}_j^+}|\mathbf{e}|\left\langle\mathbf{n}_j^{\mathbf{e}},\bar{\boldsymbol{\omega}}_{k,\mathbf{e}}\right\rangle\leq C_1^2\frac{\Delta t}{h}\frac{C_{3.5}}{\min_{\mathbf{e}\in\mathcal{T}}\sigma_{\mathbf{e}}^t h+\varepsilon}. \tag{31}$$

Collecting (30) and (31), we deduce that if:

$$\Delta t\leq\frac{h}{C_1^2}\frac{\min_{\mathbf{e}\in\mathcal{T}}\sigma_{\mathbf{e}}^t h+\varepsilon}{C_{3.5}},$$

then $I_{k,j}-\Delta t\mathcal{F}_{k,j}\geq 0$ for all (k,j). As q, $\mu^{(1)}$ and $\mu^{(2)}$ are nonnegative, we deduce that $I_{k,j}^{n+1}$ given by (19) is nonnegative.

References

[ACE+22] Pierre Anguill, Patricia Cargo, Cedric Enaux, Philippe Hoch, Emmanuel Labourasse, and Gerald Samba. An asymptotic preserving method for the linear transport equation on general meshes. *Journal of Computational Physics*, 450:110859, 2022.

[Ada01] M.L. Adams. Discontinuous finite element transport solutions in thick diffusive problems. *Nuclear Science and Engineering*, 137(3):298 – 333, 2001.

[BCWA] T S Bailey, J H Chang, J S Warsa, and M L Adams. A piecewise bi-linear discontinuous finite element spatial discretization of the sn transport equation.

[BFR16] Sebastiano Boscarino, Francis Filbet, and Giovanni Russo. High order semi-implicit schemes for time dependent partial differential equations. *Journal of Scientific Computing*, 68, 09 2016.

[BGPS88] C Bardos, F Golse, B Perthame, and R Sentis. The nonaccretive radiative transfer equations: Existence of solutions and rosseland approximation. *Journal of Functional Analysis*, 77(2):434–460, 1988.

[BH05] Thomas A. Brunner and James Paul Holloway. Two-dimensional time dependent Riemann solvers for neutron transport. *J. Comput. Phys.*, 210(1):386–399, 2005.

[BHL24] Xavier Blanc, Philippe Hoch, and Clément Lasuen. Composite finite volume schemes for the diffusion equation on unstructured meshes. *Computers and Mathematics with Applications*, 156:207–217, 2024.

[BR09] Sebastiano Boscarino and Giovanni Russo. On a class of uniformly accurate imex runge–kutta schemes and applications to hyperbolic systems with relaxation. *SIAM Journal on Scientific Computing*, 31(3):1926–1945, 2009.

[Car] B G Carlson. Transport theory: Discrete ordinates quadrature over the unit sphere.

[Cas04] John Castor. *Radiation Hydrodynamics.* Cambridge University Press, 2004.

[CDDL09] G. Carré, S. Del Pino, B. Després, and E. Labourasse. A cell-centered Lagrangian hydrodynamics scheme on general unstructured meshes in arbitrary dimension. *J. Comput. Phys.*, 228(14):5160–5183, 2009.

[CS16] F. Chaland and G. Samba. Discrete ordinates method for the transport equation preserving one-dimensional spherical symmetry in two-dimensional cylindrical geometry. *Nuclear Science and Engineering*, 182(4):417–434, 2016.

[CZ67] K.M. Case and P.F. Zweifel. *Linear Transport Theory.* Addison-Wesley series in nuclear engineering. Addison-Wesley Publishing Company, 1967.

[EG23] Alexandre Ern and Jean-Luc Guermond. Invariant-domain preserving high-order time stepping: Ii. imex schemes. *SIAM Journal on Scientific Computing*, 45(5):A2511–A2538, 2023.

[EHW21] Lukas Einkemmer, Jingwei Hu, and Yubo Wang. An asymptotic-preserving dynamical low-rank method for the multi-scale multi-dimensional linear transport equation. *Journal of Computational Physics*, 439:110353, 2021.

[Fra12] Emmanuel Franck. *Construction et analyse numérique de schema asymptotic preserving sur maillages non structurés. Application au transport linéaire et aux systèmes de Friedrichs.* PhD thesis, Université Pierre et Marie Curie - Paris VI, 2012.

[GPR20] Jean-Luc Guermond, Bojan Popov, and Jean Ragusa. Positive and asymptotic preserving approximation of the radiation transport equation. *SIAM Journal on Numerical Analysis*, 58(1):519–540, 2020.

[JL96] Shi Jin and C.David Levermore. Numerical schemes for hyperbolic conservation laws with stiff relaxation terms. *Journal of Computational Physics*, 126(2):449 – 467, 1996.

[JPT00] Shi Jin, Lorenzo Pareschi, and Giuseppe Toscani. Uniformly accurate diffusive relaxation schemes for multiscale transport equations. *SIAM Journal on Numerical Analysis*, 38(3):913–936, 2000.

[JS10] Shi Jin and Yingzhe Shi. A micro-macro decomposition-based asymptotic-preserving scheme for the multispecies boltzmann equation. *SIAM Journal on Scientific Computing*, 31(6):4580–4606, 2010.

[KFJ16] Kerstin Kupper, Martin Frank, and Shi Jin. An asymptotic preserving two-dimensional staggered grid method for multiscale transport equation. *SIAM Journal on Numerical Analysis*, 54(1):440–461, 2016.

[Kla98] Axel Klar. An asymptotic-induced scheme for nonstationary transport equations in the diffusive limit. *SIAM Journal on Numerical Analysis*, 35(3):1073–1094, 1998.

[LFH19] M. Paul Laiu, Martin Frank, and Cory D. Hauck. A positive asymptotic-preserving scheme for linear kinetic transport equations. *SIAM Journal on Scientific Computing*, 41(3):A1500–A1526, 2019.

[lM89] Edward W larsen and J.E. Morel. Asymptotic solutions of numerical transport problems in optically thick, diffusive regimes ii. *Journal of Computational Physics*, 83(1):212–236, 1989.

[LM08] Mohammed Lemou and Luc Mieussens. A new asymptotic preserving scheme based on micro-macro formulation for linear kinetic equations in the diffusion limit. *SIAM J. Scientific Computing*, 31:334–368, 01 2008.

[LM10] Jian-Guo Liu and Luc Mieussens. Analysis of an asymptotic preserving scheme for linear kinetic equations in the diffusion limit. *SIAM Journal on Numerical Analysis*, 48(4):1474–1491, 2010.

[LMM87] Edward W Larsen, J.E Morel, and Warren F Miller. Asymptotic solutions of numerical transport problems in optically thick, diffusive regimes. *Journal of Computational Physics*, 69(2):283–324, 1987.

[MM84] Dimitri Mihalas and Barbara Weibel Mihalas. *Foundations of radiation hydrodynamics.* Oxford University Press, New York, 1984.

[RJLM+88] Dautray Robert, Lions Jacques-Louis, Artola Michel, Cessenat Michel, Scheurer Bruno, and Robert Dautray. *Analyse mathématique et calcul numérique pour les sciences et les techniques . Volume 8, Évolution, semi-groupe, variationnel / Robert Dautray, Jacques-Louis Lions Michel Artola, Michel Cessenat, Bruno Scheurer.* Collection Enseignement - INSTN CEA. Masson, Paris Milan Barcelone [etc, [nouvelle édition] edition, 1988.

[Ser02] Denis Serre. Matrices: Theory and applications. 2002.